Research article

Jinxin Guo, Jialing Jian, Meng Wang, Yasuo Tomita, Lin Cao, Dayong Wang and Xinping Zhang*

Ag nanoparticle-enhanced alkyl radical generation in photopolymerization for holographic recording

https://doi.org/10.1515/nanoph-2019-0188
Received June 20, 2019; revised August 1, 2019; accepted August 16, 2019

Abstract: We report a new Ag nanoparticle-dispersed polymer nanocomposite for volume holographic recording through acrylic photopolymerization. The initial grating buildup dynamics at the inhibition stage are measured at various Ag nanoparticle concentrations. The refractive index modulation amplitude as large as 0.0069 at 633 nm is seen at the optimum Ag nanoparticle concentration of 1 wt.% with respect to the monomer. Electron paramagnetic resonance measurements show that Ag nanoparticles influence both the generation of alkyl radicals and the scavenging of oxygen in free radical photopolymerization. This mechanism intrinsically determines the molecular weight of polymer being formed and, thereby, affects the refractive index modulation amplitude of the formed grating as a function of Ag nanoparticle concentrations. Moreover, we confirm that two-beam holographic exposure leads to a periodic assembly of dispersed Ag nanoparticles using a dark-field microscopy. Our results suggest a simple way to control the photopolymerization and, therefore, to tailor polymers for practical uses.

Keywords: Ag nanoparticle; polymer; radical; holography.

1 Introduction

Holography with photopolymers has found many important applications in photonics, which include holographic data storage [1], 3D display [2], self-written waveguides [3], photolithography [4], and neutron optics [5]. In the past decade, studies of metallic nanoparticle-related physical phenomena led to an intriguing area of research. These include their unique optical properties in the visible spectral range such as surface plasmon resonance (SPR). It is known that holographic exposure in inorganic oxides/organic nanoparticle-dispersed photopolymer results in the periodic assembly of nanoparticles by the polymerization-driven mutual diffusion of the nanoparticles and monomer due to their imbalance of the chemical potentials in the bright and dark regions of an intensity-interference fringe pattern [6–8]. As a result, a volume holographic grating with a large saturated refractive modulation amplitude (Δn_{sat}) can be obtained [6–8]. Vaia et al. also demonstrated holographic assembly of Ag metallic nanoparticles in photopolymer to achieve micrometer-scale holographic patterning [9]. Goldenberg et al. also reported on holographic recording in photopolymer-dispersed with Au metallic nanoparticles (1.5–3 nm core diameter, 1–2 wt.% dispersion) [10]. They obtained Δn_{sat} as large as 0.0073 at a wavelength of 633 nm and a grating period of 980 nm. They speculated a role of Au nanoparticles during holographic recording in the promotion of the spatial segregation of monomer and an increase in Δn_{sat} as follows: (a) thiolate groups adsorbed on the surfaces of Au nanoparticles participate in the photopolymerization process as they act as chain transfer agents, which could reduce the molecular weight of growing polymers; and/or (b) Au nanoparticles can possibly terminate generating free radicals via the electron-transfer reactions. Balan et al. synthesized a polymer nanocomposite containing Ag nanoparticles that were photogenerated *in situ* by the redox process of amine radical and silver cations under holographic illumination [11]. This work provided an alternative method to manipulate the distribution of nanoparticles. Metallic nanoparticles such as Au, Ag, and Al were further used in poly(methyl methacrylate) based

***Corresponding author: Xinping Zhang,** Institute of Information Photonics Technology and College of Applied Sciences, Beijing University of Technology, Beijing 100124, China,
e-mail: zhangxinping@bjut.edu.cn.
https://orcid.org/0000-0001-6534-0004
Jinxin Guo, Jialing Jian, Meng Wang, Lin Cao and Dayong Wang: Institute of Information Photonics Technology and College of Applied Sciences, Beijing University of Technology, Beijing 100124, China
Yasuo Tomita: Department of Engineering Science, University of Electro-Communications, 1-5-1 Chofugaoka, Chofu, Tokyo 182-8585, Japan

photopolymer systems for applications in holographic data storage [12, 13] and ultrafast holography [14]. Despite the wide uses of metallic nanoparticle-dispersed polymer nanocomposites as mentioned above, a role of metallic nanoparticles in holographic recording still remains unclear. In this paper, we report on Ag nanoparticle-dispersed polymer nanocomposites that provide large Δn_{sat} with low loading of Ag nanoparticles (0.5–1.5 wt.% with respect to monomer). The Ag nanoparticles were synthesized with surface modification to ensure good solubility in the monomer blend. The effects induced by the inclusion of Ag on the photopolymerization process were quantified by the measurement of alkyl and Rose Bengal (RB) semioxidized radicals ($RB^{\bullet+}$). The mechanism of the possible increase in Δn_{sat} by the inclusion of Ag nanoparticles is discussed. In addition, the dark-field microscopy measurement was carried out in order to confirm the holographic assembly of Ag nanoparticles in the proposed polymer nanocomposites.

2 Materials and experimental section

2.1 Materials and preparation

A photoinitiator RB (0.7 wt.%) and a coinitiator N-phenylglycine (NPG, 1.4 wt.%), were added to the multifunctional monomer trimethylolpropane trimethacrylate (TMPTMA) to provide photosensitivity to green light (532 nm). All these three chemicals were obtained from Sigma Aldrich. Figure 1 shows a mechanism of photopolymerization in the Ag nanoparticle-dispersed polymer nanocomposite during exposure. When RB is exposed to green light, the ground state RB dye molecule absorbs a photon and is promoted to a singlet excited state molecule. The singlet state dye can undergo intersystem crossing into the more stable and longer-lived triplet state RB ($^3RB^*$). Then, $^3RB^*$ reacts with NPG to generate one initiation radical (aminoalkyl radical) and one reduced radical ($RB^{\bullet-}$) through the photoinduced electron transfer process, followed by the subsequent proton transfer, and the decarboxylation [15–18] as shown in Figure 1. The initiation aminoalkyl radical acts as a primary radical to initiate a growing polymer through the propagation process. $RB^{\bullet-}$ acts as a radical scavenger to inhibit the polymerization but is also able to give rise to new initiating radicals [15, 17]. $^3RB^*$ is also consumed by scavenging oxygen to generate one $RB^{\bullet+}$ [15, 19]. This oxygen scavenging process results in a reduction in the polymerization threshold at the onset of the grating buildup (*vide infra*). The chemical structures of the components used in our experiment are illustrated in Figure S1.

Ag nanoparticles were prepared by means of a modified one-step synthesis method [20]. $AgNO_3$ powder (1.7g) (Beijing Chem. Work, Beijing, China) was added to a toluene solution (40 ml) and sonicated for 30 min to attain an Ag^+ solution at a concentration of 0.25 mol/l. Decanoic acid (2.9 g) (Sigma Aldrich, St. Louis, MO, USA) was dropped into the above solution, and the mixture was stirred at a

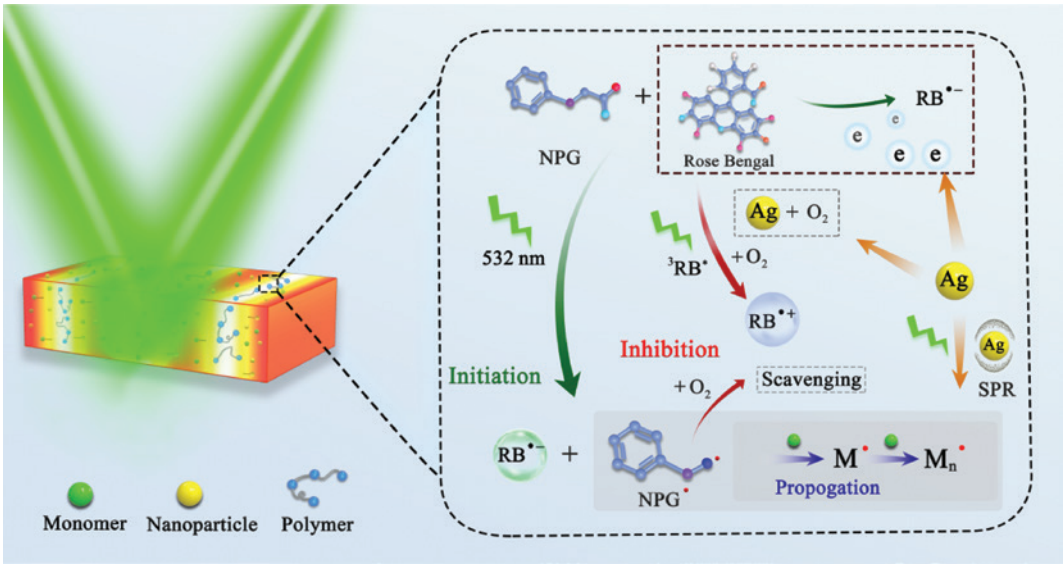

Figure 1: Schematic illustrating the mechanism of photopolymerization containing Ag nanoparticles.

temperature of 80°C for 20 min. n-Butylamine (1.67 ml) (Sigma Aldrich, St. Louis, MO, USA) was then added dropwise into the solution at the rate of 2 drops/s and mixed well by stirring. After adding aqueous hydrazine (25 ml) as a reducing agent at a rate of 2 drop/s by vigorous stirring, the solution was then constantly stirred for 4 h. The product was washed by methanol (200 ml) and precipitated in 50 ml of acetone. After centrifuging at 8000 rad/min, resuspending in methanol, precipitating, and washing with acetone, the desired dark brown Ag nanoparticles were finally obtained. The size of Ag nanoparticles varied in the range of less than 150 nm, as shown in Figure S2A.

Ag nanoparticles were dissolved in xylene at a concentration of 4.0 mg/ml. The Ag nanoparticle solution was then added to the syrup containing TMPTMA, RB, and NPG at various concentrations in wt.% with respect to the monomer and stirred thoroughly in vacuum for 3 h at room temperature until xylene evaporated. Under this processing condition, Ag nanoparticles were homogenously dispersed in the monomer blend, as shown in Figure S2A. The mixture was then casted on a 20-μm loaded quartz substrate and sandwiched with another substrate. A series of low loadings of Ag nanoparticles (0–1.5 wt.%) in the monomer blend were carried out throughout our experiment. The refractive index of the photocured mixture varied from 1.497 to 1.496, which were measured by an Abbe refractometer, at a wavelength of 633 nm at an Ag nanoparticle concentration of 0–1.5 wt.%. This means that a possible contribution of the Ag nanoparticle into Δn_{sat} is 0.001.

2.2 Holographic recording and measurements

We recorded an unslanted plane wave transmission grating at a recording intensity of 50 mW/cm^2 by two mutually coherent beams from a diode-pumped solid-state CW laser (Coherent Verdi V5, $\lambda = 532$ nm). A low intensity He-Ne laser beam ($\lambda = 633$ nm) that was insensitive to RB was employed as a Bragg-matched probe beam to monitor the grating buildup dynamics. All of the beams were *s*-polarized. We measured the time-dependent diffraction efficiency of the unslanted transmission holographic grating $\eta(t)$ defined as $I_d(t)/(I_{in} \times \text{F.C.})$, where I_d is the first-order diffracted probe beam intensity, I_{in} is the input probe beam intensity, and F.C. is the Fresnel correction factor at two substrate-air boundaries [21]. The effective thickness d was estimated by a least-squares curve fitting to the Bragg angle detuning data of $\eta(\infty)$ ($\cong \eta_{sat}$) at the saturation using the β-value method (Uchida's formalism) for an unslanted transmission grating without attenuation along the thickness direction [22]. Values for Δn_{sat} were extracted from η_{sat} with the help of Kogelnik's formula at a Bragg-matched angle and d.

2.3 Morphology characterization

Morphology experiments were performed using an FEI SIRON200 field emission scanning electron microscopy (SEM) and an FEI Talos F200 transmission electron microscopy (TEM).

2.4 Spectral characterization

An Agilent G1103A spectrophotometer was used to determine the absorption dependence on Ag doping concentration for uncured samples loaded on quartz substrates.

2.5 Electron paramagnetic resonance

Concentrations of $RB^{\bullet+}$ and alkyl radical at various concentrations of Ag nanoparticles were quantified by electron paramagnetic resonance (EPR) analysis. EPR spectra for a set of undoped and Ag nanoparticle-dispersed (0.5, 1, 1.5 wt.%) monomer blend were recorded by using a Bruker ER200-SRC-10/12 EPR spectrometer at different exposure times (5, 20, and 40 s). The corresponding concentrations of $RB^{\bullet+}$ and alkyl radicals were extracted for each sample. A LED light source (532 nm) at an intensity of 50 mW/cm^2 was used for curing the samples.

2.6 Dark-field microscopy

A Nikon DS-Fi2 microscopy combined with a fiber spectrometer (Ocean Optics USB-4000) was used for the dark-field imaging and spectral measurements to analyze uncured and grating recorded samples.

3 Results and discussion

Figure 2A shows a dependence of Δn_{sat} on Ag nanoparticle concentrations. It can be seen that there exists the optimum Ag nanoparticle concentration (1 wt.%) maximizing Δn_{sat} (0.0069). Note that each value is reproducible and was obtained as an average result following at least three separate exposures on different sample films.

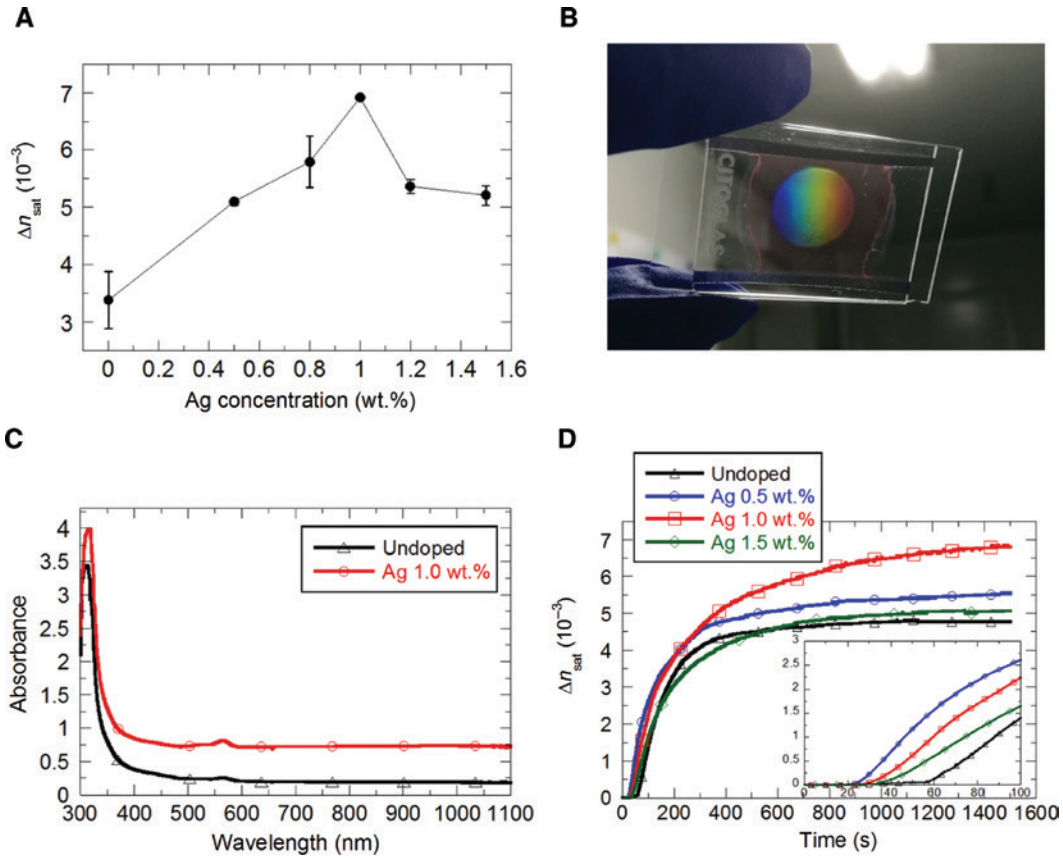

Figure 2: Characterization of holographic Ag-doped photopolymer.
(A) Dependence of Δn_{sat} on concentration of Ag nanoparticles at a grating period of 1 μm. (B) Image of a recorded grating under the white-light lamp illumination. (C) Absorptance of monomer blends with different components before exposure. (D) Buildup dynamics on Δn_{sat} of different Ag concentrations during holographic recording. Inset represents their buildup dynamics at the inhibition stage.

A photograph of a recorded grating at the Ag nanoparticle concentration of 1 wt.% is shown in Figure 2B. As mentioned in Subsection 2.1, in Ref. [10], the main possible contribution to a large Δn_{sat} could be attributed to Au nanoparticles acting as both chain transfer agents and radical terminators. Our synthesized Ag nanoparticles were functionalized by a decanoic group, which did not act as chain transfer agents for acrylic polymerization. Moreover, if Ag nanoparticles were responsible for the radical termination mechanism, it would lower the polymer conversion and, therefore, reduce Δn_{sat} [23, 24]. Hence, the reason of Ag nanoparticle-induced large Δn_{sat} in our experiment need to be further investigated.

Figure 2C illustrates the absorption spectrum of undoped and 1 wt.% Ag-doped samples. It can be seen that the inclusion of Ag nanoparticles results in a slight increase in the absorption in the visible spectral region. The absorption peak at ~560 nm is considered as the SPR, and scattering induced absorption by Ag nanoparticles embedded in the monomer blend. Ag nanoparticles bring effects on the photopolymerization process by its SPR during the holographic recording at a wavelength of 532 nm in this work [25, 26]. Furthermore, we notice that a reduction in inhibition time arises by the inclusion of Ag nanoparticles, as shown in the inset of Figure 2D. The inhibition time reduces from 58 s to 24 s by doping 0.5 wt.% and then increasing to 28 s with a further increase in Ag nanoparticles. Interestingly, a similar observation on the trend of inhibition time varying with Au nanoparticle concentration was reported [10], although it was not discussed in detail. In the holographic photopolymerization process, the inhibition time usually depends on the consumption of inhibitors (oxygens) [27]. The reduction in inhibition time implies that oxygen is consumed by Ag nanoparticles, so that the generation of $^3RB^*$ is facilitated. The increased radical generation could reduce the molecular weight of the growing polymer to promote the monomer diffusion from the dark to the bright illuminated regions and, thereby, increasing Δn_{sat}. Hence, the inclusion of Ag nanoparticles in a radical photopolymerization system could induce two major effects on the increased radical generation enhanced by SPR and/or the reaction with oxygen.

Table 1: Experimental results of $RB^{\cdot+}$ concentrations for different Ag concentrations and exposure times.

Ag concentration (wt.%)	$RB^{\cdot+}$ concentration ($\times10^{16}$) (spin/g)		
	Exposure time (s)		
	5	20	40
0	2.587	3.192	5.277
0.5	2.856	3.511	4.750
1.0	2.199	2.714	3.636
1.5	2.194	2.770	3641

Table 2: Experimental results of alkyl concentrations for different Ag concentrations and exposure times.

Ag concentration (wt.%)	Alkyl radical concentration ($\times10^{11}$) (spin/g)		
	Exposure time (s)		
	5	20	40
0	3.692	4.556	6.105
0.5	4.000	4.936	6.614
1.0	7.500	9255	12.402
1.5	6.923	8.542	11.447

In order to validate our proposed mechanism, a series of EPR measurements were carried out at varied Ag nanoparticle concentrations and exposure times. The measured EPR spectra, which indicate the characteristic peaks of $RB^{\cdot+}$ and alkyl radicals, are illustrated in Figure S3. The radical concentration can be determined by $C_R \times I/I_R$, where the C_R is the reference radical concentration for $RB^{\cdot+}$ and alkyl, I and I_R are intensities of the characteristic EPR peak of the sample and the reference, respectively. The reference concentrations of $RB^{\cdot+}$ and alkyl radicals were 1.254×10^6 and 1.000×10^6 spin/g, respectively. Tables 1 and 2 show the extracted concentrations of $RB^{\cdot+}$ and alkyl radicals from EPR spectra. It can be seen that a reduction in $RB^{\cdot+}$ occurs with increasing Ag nanoparticles. Namely, the amount of $^3RB^*$ that reacts with oxygen is reduced by Ag nanoparticles. The similar results obtained at 5 s and 20 s in 0.5 wt.% Ag nanoparticle dispersed case compared with the undoped case are considered as an influence by oxygen diffused from the air atmosphere. In the holographic recording experiment, sample films were covered by substrates to repel the replenishing oxygen from the surrounding air. However, samples in our EPR measurement were not covered, and substantial amounts of oxygen were able to diffuse into the samples at a relatively large rate compared with the case at low loading of Ag nanoparticles (0.5 wt.%) [27]. Nevertheless, the observed reduction in $RB^{\cdot+}$ concentration indicates that Ag nanoparticles suppress the reaction between $^3RB^*$ and oxygen. This leads to a reduction in the inhibition time as shown in Figure 2D and a possible increase in alkyl radicals.

Table 2 shows that an increase in alkyl concentration arises with the inclusion of Ag nanoparticles compared with the undoped case. This result indicates that the Ag nanoparticle induced photopolymerization that enhances the generation of macroradicals via the electron transfer reactions [26]. In the free radical polymerization system, the kinetic chain length related to the molecular weight of the formed polymer is defined as [23]

$$\nu = \frac{k_p[M]}{k_t[M^{\cdot}]}$$

where k_p and k_t are the rate constants of propagation and termination, respectively, and $[M]$ and $[M^{\cdot}]$ are the concentrations of monomer and growing macroradicals, respectively. An increase in macroradical concentration (i.e. alkyl radicals in the acrylic free radical polymerization process) results in a reduction in the molecular weight of the polymer and consequently facilitates the diffusion of monomer during holographic recording. However, the possible macroradical termination will increase with increasing their concentrations. Two major termination mechanisms in free radical polymerization, that is, combination and disproportionation terminations, involve the following two growing macro-radical reactions [23, 28]:

$$M_n^{\cdot} + M_m^{\cdot} \xrightarrow{k_{tc}} M_{n+m}$$

$$M_n^{\cdot} + M_m^{\cdot} \xrightarrow{k_{td}} M_n + M_m$$

where k_{tc} and k_{td} are the rate constants of the combination and disproportionation termination processes, respectively, and M_n, M_m, and M_{n+m} represent terminated chains without any radical tip, i.e. dead polymers. As the percentage of the disproportionation termination is dominant in the termination process of (meth)acrylate polymerization [23], an increase in the macroradical termination at the initial stage of holographic recording will lead to a growth in the number of oligomers. We note that diffraction signals at the early recording stage are very low as a weak volume grating being recorded is continuously refreshed in the low viscous state of the photopolymer [29]. Therefore, the inhibition time at high Ag nanoparticle concentrations (1 and 1.5 wt.%) becomes longer than that at low Ag nanoparticle concentrations (0.5 wt.%). In addition,

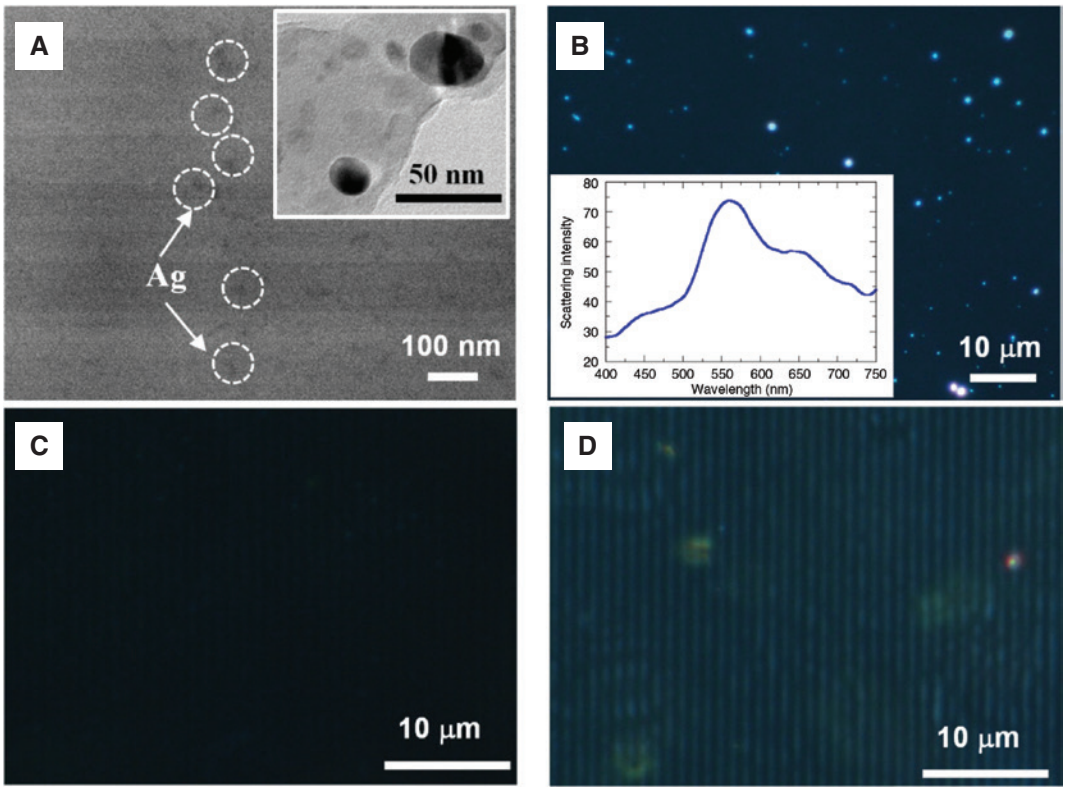

Figure 3: Morphology examinations of holographic Ag-doped photopolymer.
(A) TEM image of Ag nanoparticles at the cross section of an Ag nanoparticle-polymer composite grating. (B) Image of dark-field microscopy for 1.0 wt.% Ag-monomer blend (i.e. without RB and NPG). Inset is the scattering spectrum of Ag nanoparticles in dark field. (C) and (D) Images of dark-field microscopy of undoped and 1.0 wt.% Ag-doped gratings, respectively.

the following electron-transfer reactions to affect the inhibition process may also occur [15]:

$$RB + e \rightarrow RB^{\bullet -}$$

The Ag nanoparticle could enhance the generation f $RB^{\bullet -}$ radicals through this reaction. As mentioned in Section 2.1, $RB^{\bullet -}$ is capable of inhibiting polymerization, i.e. it results in an increase in the inhibition time. On one hand, $RB^{\bullet -}$ can produce new initiating radicals, and therefore the increase in $RB^{\bullet -}$ may also lead to a reduction in molecular weight of the growing polymer because of the premature termination induced by its inhibition [23]. Measured data shown in Tables 1 and 2 clearly show that the inclusion of Ag nanoparticles increases Δn_{sat} due to an increase in macroradical generation that is able to reduce the molecular weight of polymer and to promote the migration of unreacted monomer.

In order to characterize a volume phase grating recorded in an Ag nanoparticle-dispersed polymer composite film, we examined its morphology by TEM measurement. Figure 3A illustrates a TEM image of the cross section of a recorded grating. It can be seen that Ag nanoparticles are more likely enriched in some particular areas. It can hardly confirm the periodic distribution of Ag nanoparticles through SEM and TEM in the polymer matrix because of its relatively small size compared with the grating period. We also performed the dark-field microscopy to find light scattering from embedded Ag nanoparticles. The strong scattering of uniform distributed Ag nanoparticles in monomer blend can be easily resolved using light-scattering dark-field microscopy, as shown in Figure 3B. The obtained scattering spectrum is also consistent with the results presented in Figure 2C. The redistribution of Ag nanoparticles is easily confirmed by comparing the dark-field images of holographic grating recordings without and with Ag nanoparticles, as shown in Figure 3C and D, as similar to the case of semiconductor CdSe quantum dot-dispersed nanocomposite gratings reported previously [30].

4 Conclusions

Volume holographic recording in an Ag nanoparticle-dispersed polymer composite film was demonstrated.

We investigated an influence of varying Ag nanoparticle doping concentrations on Δn_{sat}, the generation rate of macroradicals, and the scavenging of oxygen. We showed that a small loading of Ag nanoparticles (0.5–1.5 wt.%) results in a substantive increase in Δn_{sat}. Our EPR analysis shows that the promotion of the mutual diffusion leading to an increase in Δn_{sat} is attributed to the increased macroradical generation rate and the suppression of oxygen. This result shows a new mechanism of metallic nanoparticles involving free radical photopolymerization during holographic recording. The redistribution of Ag nanoparticles due to the polymerization-driven mutual diffusion was also confirmed using dark-field microscopy. Our results are important in understanding the role of metallic nanoparticles in free radical photopolymerization and holographic recording, and are very useful for both holography and polymer synthesis uses.

Acknowledgments: J. G., D. W., and X. Z. would like to acknowledge the financial support by the National Natural Science Foundation of China (Grant Nos. Funder Id: http://dx.doi.org/10.13039/501100001809, 61605006, 61735002) and the Beijing Municipal Natural Science Foundation (Grant Nos. Funder Id: http://dx.doi.org/10.13039/501100005089, 4182013, Z180015).

References

[1] Curtis K, Dhar L, Murphy L, Hill A. Future developments, in holographic data storage: from theory to practical systems. New York: Wiley, 2010.
[2] Lu W, Xiao R, Liu J, Wang L, Zhong H, Wang Y. Large-area rainbow holographic diffraction gratings on a curved surface using transferred photopolymer films. Opt Lett 2018;43:675–8.
[3] Malallah R, Cassidy D, Muniraj I, Ryle JP, Healy JJ, Sheridan JT. Self-written waveguides in photopolymer. Appl Opt 2018;57:E80–8.
[4] Fujigaya T, Haraguchi S, Fukumaru T, Nakashima N. Development of novel carbon nanotube/photopolymernanocomposites with high conductivity and their application to nanoimprint photolithography. Adv Mater 2008;20:2151–5.
[5] Fally M, Ellabban MA, Tomita Y, et al. Neutron optical beam splitter from holographically structured nanoparticle-polymer composites. Phys Rev Lett 2010;105:123904-1–4.
[6] Suzuki N, Tomita Y, Kojima T. Volume holographic recording in TiO_2 nanoparticle-dispersed methacrylate photopolymer films. Appl Phys Lett 2002;81:4121–3.
[7] Tomita Y, Suzuki N, Chikama K. Holographic manipulation of nanoparticle distribution morphology in nanoparticle-dispersed photopolymers. Opt Lett 2005;30:839–41.
[8] Tomita Y, Hata E, Momose K, et al. Photopolymerizable nanocomposite photonic materials and their holographic applications in light and neutron optics. J Mod Opt 2016;63:S1–31.
[9] Vaia RA, Dennis CL, Natarajan LV, Tondiglia VP, Tomlin DW, Bunning TJ. One-step, micrometer-scale organization of nano- and mesoparticles using holographic photopolymerization: a generic technique. Adv Mater 2001;13:1570–4.
[10] Goldenberg LM, Sakhno OV, Smirnova TN, Helliwell P, Chechik V, Stumpe J. Holographic composites with gold nanoparticles: nanoparticles promote polymer segregation. Chem Mater 2008;20:4619–27.
[11] Balan L, Turck C, Soppera O, Vidal L, Lougnot DJ. Holographic recording with polymer nanocomposites containing silver nanoparticles photogenerated in situ by the interference pattern. Chem Mater 2009;21:5711–8.
[12] Li C, Cao L, Wang Z, Jin G. Hybrid polarization-angle multiplexing for volume holography in gold nanoparticle-doped photopolymer. Opt Lett 2014;39:6891–4.
[13] Liu Y, Fan F, Hong Y, et al. Volume holographic recording in Al nanoparticles dispersed phenanthrenequinone-doped poly(methylmethacrylate) photopolymer. Nanotechnology 2019;30:145202-1–7.
[14] Liu P, Zhao Y, Li Z, Sun X. Improvement of ultrafast holographic performance in silver nanoprisms dispersed photopolymer. Opt Express 2018;26:6993–7004.
[15] Lambert C, Sarna T, Truscotte TG. Rose bengal radicals and their reactivity. J Chem Soc Faraday Trans 1990;86:3879–82.
[16] Dong TY, Chen WT, Wang CW, et al. One-step synthesis of uniform silver nanoparticles capped by saturated decanoate: direct spray printing ink to form metallic silver films. Phys Chem Chem Phys 2009;11:6269–75.
[17] Fouassier JP, Allonas X, Burget D. Photopolymerization reactions under visible lights: principle, mechanisms and examples of applications. Prog Org Coat 2003;47:16–36.
[18] Ikeda S, Murata S. Photolysis of N-phenylglycines sensitized by polycyclic aromatic hydrocarbons: effects of sensitizers and substituent groups and application to photopolymerization. J Photochem Photobio A: Chem 2002;149:121–30.
[19] Rajesh CS, Thanulingam TL, Das S. Photoelectron transfer induced decarboxylation of substituted carboxylic acids across a liquid/liquid interface. Tetrahedron 1997;53:16817–34.
[20] Chen G, Ni M, Peng H, et al. Photoinitiation and inhibition under monochromatic green light for storage of colored 3D images in holographic polymer-dispersed liquid crystals. ACS Appl Mater Interfaces 2017;9:1810–9.
[21] O'Neill FT, Lawrence JR, Sheridan JT. Thickness variation of self-processing acrylamide-based photopolymer and reflection holography. Opt Eng 2001;40:533–9.
[22] Uchida N. Calculation of diffraction efficiency in hologram gratings attenuated along the direction perpendicular to the grating vector. J Opt Soc Am 1973;63:280–7.
[23] Odian G. Principles of polymerization, 4th ed. New York: Wiley, 1991.
[24] Gleeson MR, Guo J, Sheridan JT. Optimisation of photopolymers for holographic applications using the non-local photopolymerization driven diffusion model. Opt Express 2011;19:22423–36.
[25] Ueno K, Juodkazis S, Shibuya T, Mizeikis V, Yokota Y, Misawa H. Nanoparticle-enhanced photopolymerization. Phys Chem C 2009;113:11720–4.
[26] Deeb C, Ecoffet C, Bachelot R, Plain J, Bouhelier A, Soppera O. Plasmon-based free-radical photopolymerization: effect of

diffusion on nanolithography processes. J Am Chem Soc 2011;133:10535–42.
[27] Gleeson MR, Liu S, Guo J, Sheridan JT. Non-Local photo-polymerization kinetics including multiple termination mechanisms and dark reactions: Part III. Primary radical generation and inhibition. J Opt Soc Am B 2010;27:1804–12.
[28] Gleeson MR, Sheridan JT. Non-local photo-polymerization kinetics including multiple termination mechanisms and dark reactions: Part I. Modelling. J Opt Soc Am B 2009;26:1736–45.
[29] Kawana M, Takahashi J, Guo J, Tomita Y. Measurement of polymerization-shrinkage evolution during curing in photopolymer with a white-light Fabry-Pérot interferometer. Opt Express 2015;23:15356–64.
[30] Liu X, Tomita Y, Oshima J, et al. Holographic assembly of semiconductor CdSe quantum dots in polymer for volume Bragg grating structures with diffraction efficiency near 100%. Appl Phys Lett 2009;95:261109-1–3.

Supplementary Material: The online version of this article offers supplementary material (https://doi.org/10.1515/nanoph-2019-0188).